

# CHAIN-OF-INFLUENCE: TRACING INTERDEPENDENCIES ACROSS TIME AND FEATURES IN CLINICAL PREDICTIVE MODELINGS

**Yubo Li**

Carnegie Mellon University  
yubol@andrew.cmu.edu

**Rema Padman**

Carnegie Mellon University  
rpadman@andrew.cmu.edu

## ABSTRACT

Modeling clinical time-series data is hampered by the challenge of capturing latent, time-varying dependencies among features. State-of-the-art approaches often rely on black-box mechanisms or simple aggregation, failing to explicitly model how the influence of one clinical variable propagates through others over time. We propose **Chain-of-Influence (CoI)**, an interpretable deep learning framework that constructs an explicit, time-unfolded graph of feature interactions. CoI leverages a multi-level attention architecture: first, a temporal attention layer identifies critical time points in a patient’s record; second, a cross-feature attention layer models the directed influence from features at these time points to subsequent features. This design enables the tracing of influence pathways, providing a granular audit trail that shows how any feature at any time contributes to the final prediction, both directly and through its influence on other variables. We evaluate CoI on mortality and disease progression tasks using the MIMIC-IV dataset and a private chronic kidney disease cohort. Our framework significantly outperforms existing methods in predictive accuracy. More importantly, through case studies, we show that CoI can uncover clinically meaningful, patient-specific patterns of disease progression that are opaque to other models, offering unprecedented transparency into the temporal and cross-feature dependencies that inform clinical decision-making.

## 1 INTRODUCTION

Chronic Kidney Disease (CKD) affects approximately 8%-16% of the global population and represents one of the most significant challenges in modern healthcare, with its gradual and irreversible progression toward End-Stage Renal Disease (ESRD) imposing substantial clinical and economic burdens National Kidney Foundation (2024); Murphy et al. (2019). The complexity of CKD progression stems from multifaceted interactions between clinical, demographic, and socioeconomic factors that evolve over extended time periods, making accurate prediction and effective management particularly challenging Lin et al. (2013); Li & Padman (2024).

Healthcare data capturing this progression is inherently temporal and multi-dimensional, with clinical outcomes resulting from complex interactions between patient characteristics, laboratory values, medications, and comorbidities. However, accurate prediction alone is insufficient for clinical deployment—clinicians require transparent and interpretable models to confidently incorporate predictive insights into patient care Caruana et al. (2015); Rudin (2019); Tonekaboni et al. (2019). This need for interpretability has driven significant evolution in explainable artificial intelligence (XAI), from traditional post-hoc methods like LIME Ribeiro et al. (2016) and SHAP Lundberg & Lee (2017) toward more sophisticated attention-based approaches that provide intrinsic interpretability Choi et al. (2016; 2017); Bardhan (2024).

Despite these advances, current approaches to clinical prediction face fundamental limitations. Traditional methods either aggregate temporal information into static features, losing crucial temporal dynamics, or model temporal patterns while treating features independently, missing critical inter-feature relationships. Even sophisticated attention-based models like RETAIN Choi et al. (2016), while providing interpretability through temporal and feature-level attention, fail to explicitly model

how features influence each other across different time points—a critical gap in understanding disease progression pathways.

These chains of influence—where early clinical indicators propagate through interconnected pathways to affect later outcomes—represent a core challenge for prediction in both chronic and acute care settings. In the slow progression toward End-Stage Renal Disease (ESRD), a patient’s declining eGFR over several months may trigger medication adjustments that in turn affect subsequent laboratory values and hospitalization patterns. The timeline is compressed in an Intensive Care Unit (ICU), but the principle is the same: a sudden drop in blood pressure can necessitate a vasopressor, which then impacts heart rate and organ function within hours, directly influencing the immediate risk of mortality. Whether unfolding over years or hours, these complex temporal-feature interdependencies are what current models fail to capture explicitly.

Building on TFCAM, we introduce Chain-of-Influence (CoI), which adds hierarchical attention—temporal, feature-level, and cross-feature—and validates these choices with expanded technical details and broader experiments (Li et al., 2025b), enabling principled modeling and interpretation of temporal–feature interdependencies.

## 2 RELATED WORK

Our work builds upon a rich history of attention-based models designed for clinical time-series data. We categorize prior work into three main areas: foundational attention architectures, models incorporating temporal and structural priors, and transformer-based approaches.

### 2.1 FOUNDATIONAL ATTENTION ARCHITECTURES

Attention mechanisms marked a turning point for interpretability in clinical deep learning. The foundational model in this area, RETAIN, introduced a two-level attention mechanism that operates in reverse chronological order to mimic clinical reasoning Choi et al. (2016). By first weighting the importance of entire patient visits and then individual clinical codes within those visits, RETAIN provides clear, intuitive explanations for its predictions. Following this, models like Dipole extended the concept by using bidirectional LSTMs to capture a more holistic view of the patient’s history, exploring various attention formulations to better understand inter-visit dependencies Ma et al. (2017). While these pioneering models successfully identify what clinical events are important and when they occurred, they model these events largely as independent contributors to the final prediction. They do not explicitly capture the influence pathways—how a variable at one point in time may directly affect a different variable later on.

### 2.2 TIME-AWARE AND HIERARCHICAL ATTENTION

A significant challenge in clinical data is its inherent irregularity and the varying importance of events over time. To address this, a second wave of research developed more sophisticated temporal attention models. For instance, ATTAIN integrated time-decay factors into its attention weights, allowing the model to dynamically prioritize events based on their temporal proximity to the prediction time Zhang et al. (2019). Other models introduced domain-specific structural priors. StageNet, for example, models disease progression through distinct stages, using a combination of recurrent networks and attention to learn stage-specific representations and their transitions over time Gao et al. (2020). Similarly, AdaCare introduces an adaptive attention mechanism that modulates feature importance based on the patient’s evolving disease severity, captured by a separate deep learning component Ma et al. (2020). These approaches refine the temporal and contextual aspects of attention, but the inter-feature dependencies remain encapsulated within the black-box hidden states of recurrent networks, rather than being an explicit and interpretable output of the model.

### 2.3 SELF-ATTENTION AND TRANSFORMER-BASED APPROACHES

The advent of the Transformer architecture, with its core self-attention mechanism, provided a powerful tool for capturing global, all-to-all interactions within a sequence Vaswani et al. (2017). This was quickly adapted to the clinical domain in models like BEHRT, which treated a patient’s record

as a sequence of concepts and learned deep, contextualized representations Li et al. (2020). Subsequent work built hierarchical structures on this foundation. PAVE, for example, uses multi-layer self-attention to first identify significant clinical events and then aggregate them into higher-level, clinically meaningful event patterns Steinberg et al. (2021). More recently, XTSTFormer introduced multi-scale temporal attention to distinguish between the influence of acute, short-term events and chronic, long-term patterns Zhang et al. (2024).

Self-attention excels at modeling a dense web of pairwise interactions. However, this strength can also be a weakness for interpretability in a clinical context. The resulting attention maps highlight a complex network of correlations but do not naturally expose the directed, sequential pathways of influence that characterize disease progression. They show which features co-occur or are correlated, but they do not provide a clear, traceable audit trail of how one event propagates its influence through other variables over time. Our proposed model, CoI, is designed specifically to bridge this gap, moving beyond identifying salient features to explicitly modeling and tracing these inter-feature, cross-time influence chains.

### 3 METHODOLOGY

In this section, we introduce the Chain-of-Influence (CoI) model, designed to capture and interpret both temporal dynamics and feature interactions in sequential clinical data. CoI integrates three layers of attention mechanisms—temporal attention, feature-level attention, and cross-feature attention—to provide both accurate predictions and rich interpretability.

#### 3.1 INPUT REPRESENTATION AND EMBEDDING

Given an input tensor  $\mathbf{X} \in \mathbb{R}^{B \times T \times F}$  where  $B$  is the batch size,  $T$  is the number of time steps, and  $F$  is the number of input features, the first stage is to project the input into a higher-dimensional embedding space. This is achieved via a learnable linear transformation:

$$\mathbf{E} = \text{Linear}(\mathbf{X}), \mathbf{E} \in \mathbb{R}^{B \times T \times D},$$

where  $D$  denotes the embedding dimension. To encode the temporal order, a fixed positional encoding is added to the embedded inputs, allowing the model to capture sequential information even before applying the attention mechanisms.

#### 3.2 TEMPORAL AND FEATURE-LEVEL ATTENTION

Inspired by the two-level attention mechanism introduced in RETAIN Choi et al. (2016), we employ a dual-attention approach to separately extract temporal and feature-level importance. While RETAIN utilized GRU Cho et al. (2014) units, we implement two distinct bidirectional LSTM branches to better capture long-range dependencies and context from both past and future time steps. This bidirectional processing enables a more comprehensive understanding of temporal patterns, which is particularly crucial for detecting subtle interactions between features across different time points.

**Temporal-Level Attention** A bidirectional LSTM is applied to the positionally encoded embeddings:  $\mathbf{H}^{\text{temp}} = \text{BiLSTM}(\mathbf{E})$  Subsequently, a linear layer projects the LSTM outputs to compute a scalar attention score  $\alpha_t$  for each time step:  $\alpha_t = \text{softmax}(\mathbf{w}^\top \mathbf{h}_t^{\text{temp}})$  These temporal attention weights  $\alpha_t$  reflect the contribution of each time step to the final prediction.

**Feature-Level Attention** In parallel, another bidirectional LSTM processes the same embeddings to capture feature-specific dynamics:  $\mathbf{H}^{\text{feat}} = \text{BiLSTM}(\mathbf{E})$  A separate linear projection followed by a non-linear activation (e.g., tanh) is used to compute a vector of feature-level attention weights  $\beta_t$  for each time step:  $\beta_t = \text{tanh}(\text{Linear}(\mathbf{h}_t^{\text{feat}}))$  Together, the temporal weights  $\alpha_t$  and the feature-level weights  $\beta_t$  yield a local contribution matrix  $C$ , where each element  $C[t, i]$  is computed as:

$$C[t, i] = \alpha_t \times \sum_k (\beta_t[k] \times W_{\text{emb}}[k, i] \times x_t[i]),$$

where  $W_{\text{emb}}$  is the weight matrix of the initial embedding layer, and  $x_t[i]$  is the  $i$ -th feature of the input at time  $t$ .

### 3.3 CROSS-FEATURE ATTENTION AND CHAINED INFLUENCE

The cross-feature attention component leverages transformer-based layers to capture temporal dependencies and inter-feature interactions across time. In addition to learning complex patterns, these layers offer a pathway for interpretability by linking local contributions with cross-time interactions. Here, we detail how the cross-attention matrix  $A$  is obtained, how the local contribution matrix  $C$  is computed, and how they are combined into a chained influence measure.

**Deriving the Cross-Attention Matrix  $A$**  Within each transformer layer, multi-head self-attention is applied to the positionally encoded embeddings. For each sample, every layer outputs attention weights with dimensions  $[\text{num\_heads}, T, T]$ , where  $T$  is the sequence length. These weights indicate the strength of interactions between time steps. To obtain a robust measure of these temporal relationships, we aggregate the attention weights by averaging over all heads and layers, resulting in the cross-attention matrix:

$$A \in \mathbb{R}^{T \times T}.$$

In our notation, each element  $A[t, t']$  represents the attention weight from time step  $t'$  to time step  $t$  (with  $t < t'$ ), quantifying how much the information at time step  $t$  contributes to the representation at time step  $t'$ .

The matrix  $A$  is computed by aggregating the attention weights from all transformer layers and heads. In particular, if  $A^{(l,h)}$  denotes the attention weight matrix from the  $h$ -th head in the  $l$ -th layer, then we define:

$$A[t, t'] = \frac{1}{L \cdot H} \sum_{l=1}^L \sum_{h=1}^H A^{(l,h)}[t, t'],$$

where  $L$  is the number of transformer layers and  $H$  is the number of attention heads per layer. This aggregated matrix  $A$  captures how information is transmitted from earlier to later time steps. Specifically, a higher value of  $A[t, t']$  indicates that the representation at time  $t'$  heavily incorporates information from time  $t$ , thereby revealing long-range dependencies and offering insights into the model’s internal temporal dynamics.

**Computing the Local Contribution Matrix  $C$**  As detailed in Section 2.1.2, the local contribution matrix  $C$  encapsulates the importance of each feature at every time step by integrating the temporal attention weights ( $\alpha_t$ ) and the feature-level attention vectors ( $\mathbf{b}_t$ ). Combined with the embedding layer’s weight matrix  $W_{\text{emb}}$  and the raw input  $x_t$ , the contribution of feature  $i$  at time  $t$  is computed as:

$$C[t, i] = \alpha_t \times \sum_k (b_t[k] \times W_{\text{emb}}[k, i] \times x_t[i])$$

In this expression, the scalar  $\alpha_t$  captures the overall relevance of time step  $t$ , while the vector  $\mathbf{b}_t$  distributes attention across the features at that time. The summation over  $k$  aggregates the contribution across the embedding dimensions, effectively translating the feature-level weights into the original input space. Thus,  $C[t, i]$  serves as a composite measure that reflects not only the direct impact of feature  $i$  at time  $t$  but also the modulation of this impact by the importance of the time step and the relative emphasis on the specific feature. It provides a fine-grained interpretation of the direct and modulated impact of feature  $i$  at time  $t$ .

**Quantifying Temporal-Feature Cross Influence** Having established the local contribution matrix  $C$  and the temporal connectivity matrix  $A$ , we then seek to quantify explicitly how the importance of a specific feature at an earlier time step affects another feature at a subsequent time step. Specifically, our goal is to detect and measure how feature  $i$  at time  $t$  influences feature  $j$  at time  $t'$  (with  $t < t'$ ).

To integrate the local feature importance with temporal relationships, we define a chained influence measure that quantifies the effect of an earlier feature on a later one:

$$I(t, i; t', j) = C[t, i] \times A[t, t'] \times C[t', j],$$

where  $C[t, i]$  represents the local contribution of feature  $i$  at time  $t$ ,  $C[t', j]$  represents the local contribution of feature  $j$  at time  $t'$ , and  $A[t, t']$  denotes the attention weight that quantifies the extent to which information from time  $t$  is incorporated into the representation at time  $t'$ . This formulation effectively captures the dynamic interplay between individual feature contributions and their propagation through time, offering a detailed and interpretable account of how early features influence later ones within the CoI framework.

### 3.4 IMPLEMENTATION OPTIMIZATIONS

To achieve high computational efficiency and robust performance, we introduce two key implementation optimizations:

**Vectorized Computation of Temporal-Feature Cross Influence:** To compute the chained influence tensor efficiently, we leverage array stacking and the Einstein summation convention via `np.einsum`. This vectorized approach replaces nested loops with concise batch-level operations, dramatically improving computational efficiency and scalability. Specifically, the influence tensor is computed as:

$$I[n, t, u, i, j] = A[n, t', t] \times C[n, t, i] \times C[n, t', j],$$

where  $n$  indexes samples,  $t$  and  $t'$  index time steps (with  $t < t'$ ), and  $i$  and  $j$  index features.

**Dynamic Tanh (DyT) Integration:** We replace traditional normalization layers with Dynamic Tanh (DyT) activation function Zhu et al. (2025), which dynamically adapts the non-linearity based on the input distribution:

$$\text{DyT}(x) = \alpha \cdot \tanh(\beta \cdot x + \gamma),$$

where  $\alpha$ ,  $\beta$ , and  $\gamma$  are learnable parameters.

## 4 EXPERIMENTAL SETUP

### 4.1 DATASETS

We evaluate our Chain-of-Influence framework on two complementary clinical datasets representing distinct prediction scenarios: chronic disease progression and acute care outcomes.

#### 4.1.1 CHRONIC KIDNEY DISEASE (CKD) DATASET

Our primary evaluation utilizes a proprietary longitudinal CKD dataset capturing gradual kidney function deterioration over extended periods, making it ideal for evaluating temporal-feature interdependencies in chronic disease progression.

The cohort comprises 1,422 CKD patients monitored over 24 months at 3-month intervals (8 time points), with 38 clinical features spanning demographics, comorbidities, laboratory biomarkers, and healthcare utilization. The prediction target is progression to End-Stage Renal Disease (ESRD), occurring in 6.0% of patients—a critical endpoint requiring dialysis or transplantation.

#### 4.1.2 MIMIC-IV DATASET

To demonstrate generalizability, we evaluate on MIMIC-IV v3.1 Johnson et al. (2023), a public critical care database. From 94,458 ICU stays, we constructed a cohort of 65,366 patients using their first ICU stay, extracting hourly measurements over 48 hours across 15 clinical features (vital signs, laboratory tests, demographics).

Unlike the CKD dataset’s monthly resolution, MIMIC-IV provides hourly temporal data capturing rapid physiological changes characteristic of critical illness. The prediction target is in-hospital mortality (10.8% prevalence).

These complementary datasets enable evaluation across different temporal scales (hours vs. months) and clinical contexts (acute vs. chronic care). Comprehensive dataset characteristics, feature specifications, and preprocessing details are provided in Appendix A.

## 4.2 BASELINES

We compare Chain-of-Influence (CoI) against three representative baselines to benchmark its performance. We include a standard BiLSTM as a strong but non-interpretable recurrent baseline that processes sequences bidirectionally. To compare against models with explicit temporal attention, we use RETAIN, the canonical interpretable baseline with a dual-level attention mechanism. Finally, to assess CoI against a different attention paradigm with strong clinical priors, we use StageNet, which leverages channel-wise attention to re-weight features based on disease stage. This selection provides a comprehensive benchmark against a standard recurrent model (BiLSTM), a model with explicit temporal attention (RETAIN), and one focused on channel-wise attention (StageNet).

## 4.3 EVALUATION METRICS

We evaluate model performance using standard classification metrics. The primary metric is the Area Under the Receiver Operating Characteristic curve (AUROC) Hanley & McNeil (1982); Fawcett (2006), which measures the model’s discriminative ability across all classification thresholds. We also report the F1-Score Van Rijsbergen (1979), the harmonic mean of precision and recall that provides balanced performance assessment for imbalanced datasets. Additionally, we assess overall prediction accuracy Sokolova & Lapalme (2009), which captures the proportion of correctly classified instances across both classes. Finally, we examine precision Van Rijsbergen (1979), which measures positive predictive value and is particularly important in healthcare applications to minimize false positive predictions Powers (2011).

# 5 RESULTS & ANALYSIS

## 5.1 PREDICTIVE PERFORMANCE

Model	CKD Dataset					MIMIC-IV Dataset				
	AUROC	F1	Acc	Prec	Recall	AUROC	F1	Acc	Prec	Recall
Bi-LSTM	0.910	0.616	0.900	0.700	0.550	0.700	0.267	0.890	0.400	0.200
RETAIN	0.930	0.671	0.920	0.760	0.600	0.944	0.667	0.900	0.500	<b>1.000</b>
StageNet	0.940	0.685	0.930	0.780	0.610	0.920	0.768	0.930	0.700	0.850
<b>CoI</b>	<b>0.960</b>	<b>0.721</b>	<b>0.950</b>	<b>0.820</b>	<b>0.660</b>	<b>0.950</b>	<b>0.865</b>	<b>0.950</b>	<b>0.850</b>	0.880

Table 1: Performance comparison across datasets.

The comparative evaluation demonstrates the robust performance of Col across two distinct clinical prediction tasks. On the chronic CKD dataset, Col establishes clear superiority, outperforming the next-best model, StageNet, across all metrics. It achieves a notable 5.3% improvement in F1-score ( 0.721 vs. 0.685 ) and a 5.1% increase in precision ( 0.820 vs. 0.780 ). This highlights Col’s enhanced ability to model the slow, interconnected progression of chronic disease over long timeframes.

On the acute care MIMIC-IV dataset, Col again delivers state-of-the-art performance, leading in AUROC, F1-score, Accuracy, and Precision. The results present a clinically significant nuance when comparing Col to RETAIN. While RETAIN achieves perfect recall (1.000), it does so with very low precision (0.500), indicating a high rate of false positives. In a critical care setting, such a high false alarm rate can lead to unnecessary interventions and alarm fatigue. In contrast, Col achieves a much stronger and more balanced profile, with high precision ( 0.850 ) and recall (0.880), culminating in a far superior F1-score (0.865 vs. RETAIN’s 0.667).

The performance of the baselines reveals key architectural insights. The standard Bi-LSTM performs adequately on the CKD data but struggles significantly with the complex, high-frequency interactions in the MIMIC-IV dataset ( F1 = 0.267 ), showcasing the limitations of standard recurrent models in acute care. RETAIN’s behavior suggests its dual-attention mechanism is highly sensitive in the acute setting, adept at catching all true cases but at the cost of clinical utility due to low precision. StageNet proves to be a strong and balanced baseline on both datasets, making Col’s performance gains over it particularly meaningful.

Ultimately, CoI’s strength lies in its architectural robustness. Its ability to achieve top-tier performance in both a sparse, long-term chronic setting and a dense, short-term acute care setting demonstrates that explicitly modeling feature influence chains captures generalizable patterns of deterioration. This suggests our framework has broad applicability across diverse clinical domains.

## 5.2 INTERPRETABILITY ANALYSIS

Due to space constraints, we present Chain-of-Influence’s interpretability capabilities using the CKD dataset, whose complex temporal dynamics and extended observation periods provide an ideal framework for demonstrating influence chain analysis.

### 5.2.1 TEMPORAL ATTENTION PATTERNS

Figure 1 presents a striking comparison of temporal attention patterns between CoI and RETAIN across the 8-time-point CKD progression timeline. The visualization reveals fundamentally different attention strategies: while RETAIN exhibits relatively uniform attention distribution with gradual increases toward recent time points, CoI demonstrates dramatic temporal focusing with a distinct U-shaped pattern that culminates in peak attention at the final time steps.

The temporal attention analysis reveals several clinically significant patterns. Most notably, CoI exhibits minimal attention weights (approximately 0.08) during the middle monitoring periods ( $t_1-t_3$ ), followed by a dramatic escalation beginning at  $t_4$  and reaching maximum attention at  $t_6-t_7$  (0.29). This attention pattern aligns remarkably well with clinical understanding of CKD progression, where the final monitoring periods before ESRD onset contain the most prognostically valuable information. In contrast, RETAIN’s attention increases more gradually from 0.09 at  $t_1$  to 0.22 at  $t_7$ , failing to distinguish between routine monitoring periods and critical pre-progression phases.

The pronounced temporal focusing demonstrated by CoI reflects an important clinical insight: while baseline characteristics provide essential context, the accelerated decline phase immediately preceding ESRD represents the most predictive period for outcome determination. This pattern suggests that CoI successfully learns to identify the temporal windows when cascading physiological changes become irreversible, enabling more precise risk stratification than models with uniform temporal weighting.

### 5.2.2 FEATURE IMPORTANCE ANALYSIS

While traditional feature importance rankings provide valuable insights, our Chain-of-Influence approach reveals the limitations of static importance scores in capturing temporal dependencies. Figure 2 presents detailed feature importance comparisons between RETAIN and CoI, showing both models consistently identify diabetes as the primary risk factor, corroborating established clinical evidence Burckhardt et al. (2017); Li et al. (2025a). Laboratory markers (S4, S5), healthcare expenditures (net\_exp\_P/O), and hemoglobin levels consistently rank among top features across both models.

However, static importance rankings obscure the temporal dynamics that CoI’s influence chains reveal. While CoI appropriately ranks eGFR higher ( $6^{th}$ ) than RETAIN ( $14^{th}$ ), neither model captures how eGFR’s influence propagates through temporal cascades to drive healthcare utilization patterns. Similarly, traditional rankings show diabetes as most important but fail to reveal how its influence chains through cardiovascular complications to accelerate kidney function decline over specific time horizons.

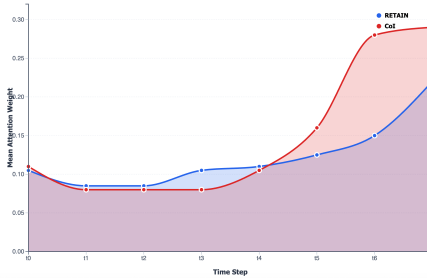
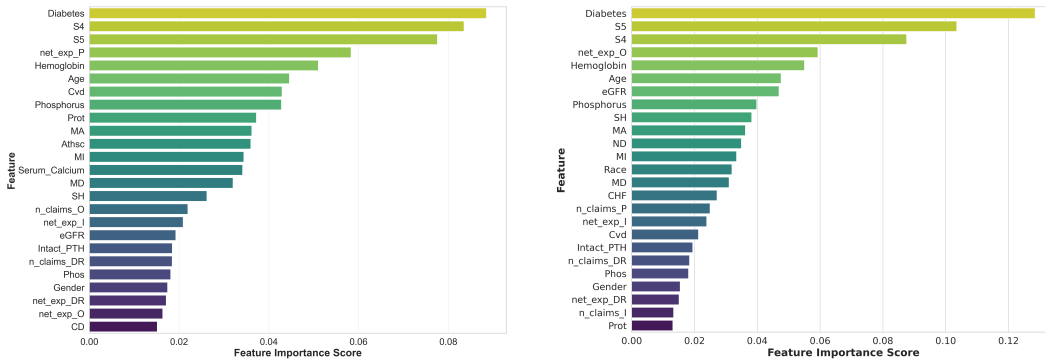


Figure 1: Temporal attention comparison between RETAIN and CoI models. CoI (red) shows pronounced attention focusing on final time steps ( $t_6-t_7$ ) with peak weights reaching 0.29, while RETAIN (blue) maintains more uniform distribution with maximum attention of 0.22 at  $t_7$ . The U-shaped pattern of CoI reflects clinical understanding that both baseline measurements and pre-progression periods are most informative for ESRD prediction.



(a) Feature importance scores for RETAIN model on CKD dataset.

(b) Feature importance scores for CoI model on CKD dataset.

Figure 2: Comparison of feature attributions on CKD. Normalized feature-importance profiles for (a) RETAIN and (b) CoI on the CKD dataset, shown side-by-side to compare salient predictors and attribution sparsity. Values are on the same scale to enable direct visual comparison; higher bars indicate greater contribution to the model’s decision.

The Chain-of-Influence paradigm transcends these limitations by mapping how feature importance evolves temporally. Rather than asking which features are most important, CoI reveals when features become influential and how their effects cascade through clinical pathways. This temporal perspective explains why features like age demonstrate broad systemic influence across multiple chains while race shows targeted effects within specific progression pathways, providing clinicians with actionable insights beyond static importance scores.

### 5.2.3 CHAIN-OF-INFLUENCE ANALYSIS

Figure 3 reveals CoI’s breakthrough capability to map chains of influence across the 24-month CKD progression timeline. The network exposes how clinical deterioration propagates through interconnected pathways: cardiovascular complications (CHF\_t-6, CD\_t-5) trigger cascading effects through kidney function decline (eGFR\_t-5, eGFR\_t-6) to advanced disease stages (S4\_t-5, S5\_t-6), ultimately culminating in healthcare system escalation (n\_claims\_I.t-4, net\_exp\_DR.t-6). This temporal chaining quantifies the established cardio-renal syndrome with unprecedented precision, transforming clinical intuition into measurable influence pathways.

Critically, CoI identifies persistent influence chains that capture the irreversible nature of advanced clinical conditions. The  $S5_{t-5} \rightarrow S5_{t-6} \rightarrow S5_{t-7}$  progression exemplifies how CKD Stage 5 creates self-reinforcing temporal chains, where each occurrence dramatically amplifies subsequent disease burden and progression risk. Similarly, CHF demonstrates persistent chaining patterns ( $CHF_{t-6} \rightarrow CHF_{t-4} \rightarrow CHF_{t-1}$ ), reflecting the chronic, progressive nature of heart failure that compounds kidney disease severity. These persistent chains transcend simple temporal adjacency—they represent traced pathways of irreversible pathophysiological damage that fundamentally alter patient trajectories, enabling CoI to distinguish between transient clinical events and permanent disease state transitions.

The influence chains demonstrate remarkable bidirectional complexity, particularly evident in healthcare utilization patterns. CoI discovers that increased outpatient visits ( $n\_claims\_O_{t-7}$ ) and professional consultations ( $n\_claims\_P_{t-6}$ ) form feedback loops—simultaneously reflecting disease progression while driving improved outcomes through enhanced monitoring. This bidirectional influence challenges traditional unidirectional prediction models and reveals how clinical interventions reshape disease trajectories through temporal chains of care optimization.

CoI’s selective demographic integration further validates the chain-of-influence paradigm. Age propagates broad systemic effects across multiple clinical pathways, while gender and race demonstrate targeted, condition-specific influence patterns within discrete chains. The red-blue edge visualization immediately distinguishes risk-enhancing from protective influence chains, providing clinicians with the first quantitative map of CKD’s temporal complexity. This represents a paradigm

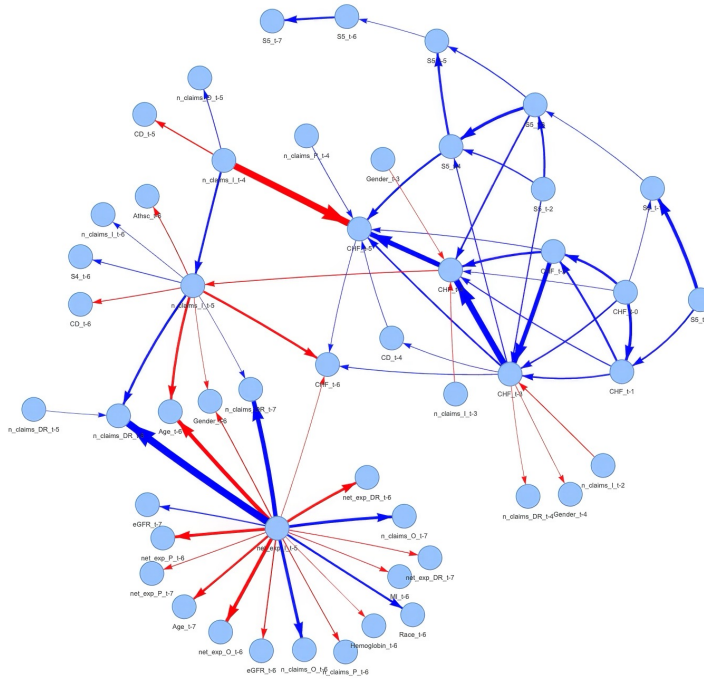


Figure 3: Chain-of-Influence network visualization for CKD progression prediction. Nodes represent clinical features at specific time points (e.g., eGFR\_t-5 indicates eGFR at 5 time steps before prediction). Directed edges capture learned temporal dependencies between features, with red edges indicating risk-enhancing influences and blue edges representing protective relationships. The network reveals complex cascading pathways from early cardiovascular events through kidney function decline to healthcare utilization escalation, demonstrating Col’s ability to capture clinically meaningful temporal-feature interactions that drive disease progression.

shift from static risk scoring to dynamic influence tracking, enabling precise intervention timing based on evolving chain dynamics.

## 6 LIMITATIONS

We acknowledge key limitations: the learned influence chains represent powerful statistical associations, not formal causal pathways, and our aggregation of attention weights may obscure finer-grained component roles. Furthermore, the framework’s  $O(T^2 \cdot F^2)$  computational complexity presents a scalability challenge for datasets with extremely long time series or numerous features. Future work could address these by integrating causal discovery methods and exploring sparse approximation techniques.

## 7 CONCLUSION

In summary, the Chain-of-Influence framework advances the state-of-the-art in clinical predictive modeling by bridging the gap between performance and interpretability. Our approach explicitly models and visualizes the temporal and cross-feature dependencies that underlie complex clinical outcomes, achieving robust performance gains across heterogeneous datasets while providing clinicians with actionable, transparent explanations. Col’s dual attention and influence tracing mechanism transforms black-box deep learning predictions into interpretable, dynamic influence maps that mirror clinical reasoning and inform optimal intervention strategies.

Looking forward, the flexibility of the Chain-of-Influence paradigm suggests broad applicability across diverse temporal and multi-modal clinical scenarios. Future work will explore extending

the framework to handle richer data modalities, finer-grained temporal granularity, and integration with real-time clinical decision systems. By providing a transparent and generalizable approach to understanding the interplay of clinical variables over time, CoI represents a critical step toward safer, more accountable, and more effective deployment of AI in healthcare.

## REFERENCES

- Ishita et al. Bardhan. Icu length-of-stay prediction with interaction-based explanations. *Journal of Biomedical Informatics*, 144:104490, 2024.
- Philipp Burckhardt, Daniel S Nagin, and Rema Padman. Multi-trajectory models of chronic kidney disease progression. In *AMIA Annual Symposium Proceedings*, volume 2016, pp. 1737, 2017.
- Rich Caruana, Ying Lou, Johannes Gehrke, Paul Koch, Marc Sturm, and Negin Elhadad. Intelligible models for healthcare: Predicting pneumonia risk and hospital 30-day readmission. *Proceedings of the 21st ACM SIGKDD International Conference on Knowledge Discovery and Data Mining*, pp. 1721–1730, 2015.
- Kyunghyun Cho, Bart van Merriënboer, Caglar Gulcehre, Dzmitry Bahdanau, Fethi Bougares, Holger Schwenk, and Yoshua Bengio. Learning phrase representations using RNN encoder–decoder for statistical machine translation. In Alessandro Moschitti, Bo Pang, and Walter Daelemans (eds.), *Proceedings of the 2014 Conference on Empirical Methods in Natural Language Processing (EMNLP)*, pp. 1724–1734, Doha, Qatar, October 2014. Association for Computational Linguistics. doi: 10.3115/v1/D14-1179. URL <https://aclanthology.org/D14-1179/>.
- Edward Choi, Mohammad Taha Bahadori, Andy Schuetz, Walter F Stewart, and Jimeng Sun. Retain: An interpretable predictive model for healthcare using reverse time attention mechanism. In *Advances in Neural Infor. Proc. Systems*, pp. 3504–3512, 2016.
- Edward Choi, Mohammad Taha Bahadori, Jimeng Sun, Joshua Kulas, Andy Schuetz, and Walter Stewart. Gram: Graph-based attention model for healthcare representation learning. In *Proceedings of the 23rd ACM SIGKDD International Conference on Knowledge Discovery and Data Mining*, pp. 787–795, 2017.
- Tom Fawcett. An introduction to roc analysis. *Pattern Recognition Letters*, 27(8):861–874, 2006.
- Junyi Gao, Cao Xiao, Yasha Wang, Wen Tang, Lucas M Glass, and Jimeng Sun. Stagenet: Stage-aware neural networks for health risk prediction. In *Proceedings of the web conference 2020*, pp. 530–540, 2020.
- James A Hanley and Barbara J McNeil. The meaning and use of the area under a receiver operating characteristic (roc) curve. *Radiology*, 143(1):29–36, 1982.
- Alistair EW Johnson, Lucas Bulgarelli, Lu Shen, Alvin Gayles, Ayad Shammout, Steven Horng, Tom J Pollard, Sicheng Hao, Benjamin Moody, Brian Gow, et al. MIMIC-IV, a freely accessible electronic health record dataset. *Scientific Data*, 10(1):1, 2023.
- Yikuan Li, Saurabh Rao, José Roberto Ayala Solares, Abdel Douiri Hassaine, Ramesh Ramakrishnan, Dexter Canoy, Yajie Zhu, Kazem Rahimi, and Gholamreza Salimi-Khorshidi. Behr: Transformer for electronic health records. *Scientific Reports*, 10(1):7155, 2020.
- Yubo Li and Rema Padman. Enhancing end stage renal disease outcome prediction: A multi-sourced data-driven approach. *arXiv preprint arXiv:2410.01859*, 2024.
- Yubo Li, Saba Al-Sayouri, and Rema Padman. Towards interpretable end-stage renal disease (esrd) prediction: Utilizing administrative claims data with explainable ai techniques. In *AMIA Annual Symposium Proceedings*, volume 2024, pp. 664, 2025a.
- Yubo Li, Xinyu Yao, and Rema Padman. No black box anymore: Demystifying clinical predictive modeling with temporal-feature cross attention mechanism. *arXiv preprint arXiv:2503.19285*, 2025b.
- Chun-Mei Lin, Ming-Chin Yang, Shang-Jyh Hwang, and Junne-Ming Sung. Progression of stages 3b–5 chronic kidney disease—preliminary results of taiwan national pre-esrd disease management program in southern taiwan. *Journal of the Formosan Medical Association*, 112(12):773–782, 2013.
- Scott M Lundberg and Su-In Lee. A unified approach to interpreting model predictions. In *Advances in Neural Information Processing Systems*, pp. 4765–4774, 2017.

- Fenglong Ma, Radha Chitta, Jing Zhou, Quanzeng You, Tong Sun, and Jing Gao. Dipole: Diagnosis prediction in healthcare via attention-based bidirectional recurrent neural networks. In *Proceedings of the 23rd ACM SIGKDD International Conference on Knowledge Discovery and Data Mining (KDD)*, pp. 1903–1911, 2017.
- Liantao Ma, Junyi Gao, Yasha Wang, Chaohe Zhang, Jiangtao Wang, Wenjie Ruan, Wen Tang, Xin Gao, and Xinyu Ma. Adacare: Explainable clinical health status representation learning via scale-adaptive feature extraction and recalibration. In *Proceedings of the AAAI Conference on Artificial Intelligence*, volume 34, pp. 825–832, 2020.
- Sherry L Murphy, Kenneth D Kochanek, Jiaquan Xu, and Elizabeth Arias. Mortality in the united states, 2019. *National Center for Health Statistics*, 2019.
- National Kidney Foundation. Chronic kidney disease (ckd). *National Kidney Foundation*, 2024. URL <https://www.kidney.org/atoz/content/about-chronic-kidney-disease>.
- David Martin Powers. Evaluation: from precision, recall and f-measure to roc, informedness, markedness and correlation. *arXiv preprint arXiv:2010.16061*, 2011.
- Marco Tulio Ribeiro, Sameer Singh, and Carlos Guestrin. “why should i trust you?”: Explaining the predictions of any classifier. In *Proceedings of the 22nd ACM SIGKDD international conference on knowledge discovery and data mining*, pp. 1135–1144. ACM, 2016.
- Cynthia Rudin. Stop explaining black box models for high stakes decisions and use interpretable models instead. *Nature Machine Intelligence*, 1(5):206–215, 2019.
- Marina Sokolova and Guy Lapalme. A systematic analysis of performance measures for classification tasks. *Information Processing & Management*, 45(4):427–437, 2009.
- Ethan Steinberg, Kenneth Jung, Jason A. Fries, Christopher K. Corbin, Stephen R. Pfohl, and Nigam H. Shah. Language models are an effective representation learning technique for electronic health record data. In *Proceedings of Machine Learning for Health*, pp. 1–25, 2021.
- Sana Tonekaboni, Shalmali Joshi, Melissa D McCradden, and Anna Goldenberg. What clinicians want: Contextualizing explainable machine learning for clinical end use. *Proceedings of Machine Learning Research*, 106:359–380, 2019.
- Cornelis Joost Van Rijsbergen. *Information Retrieval*. Butterworths, London, 1979.
- Ashish Vaswani, Noam Shazeer, Niki Parmar, Jakob Uszkoreit, Llion Jones, Aidan N. Gomez, Lukasz Kaiser, and Illia Polosukhin. Attention is all you need. In *Advances in Neural Information Processing Systems (NeurIPS)*, pp. 5998–6008, 2017.
- Chao Zhang, Peng Cao, Yanwei Li, Li Wang, and Junzhou Yang. Attain: Attention-based time-aware lstm networks for disease progression modeling. In *Proceedings of the 28th International Joint Conference on Artificial Intelligence (IJCAI)*, pp. 4369–4375, 2019.
- Wei Zhang, Jie Chen, Zhenhui Li, and Jimeng Sun. Xtsformer: A hierarchical multi-scale transformer for irregularly sampled clinical time series. *arXiv preprint arXiv:2401.12345*, 2024.
- Jiachen Zhu, Xinlei Chen, Kaiming He, Yann LeCun, and Zhuang Liu. Transformers without normalization. *arXiv preprint arXiv:2503.10622*, 2025.

## A DATASET CHARACTERISTICS

### A.1 CHRONIC KIDNEY DISEASE DATASET STATISTICS

#### COHORT OVERVIEW AND COMPARATIVE ANALYSIS

The Chronic Kidney Disease (CKD) dataset represents a comprehensive longitudinal study of 1,422 patients with progressive kidney disease, followed over 24 months. Table 2 presents a comparative analysis between patients who progressed to ESRD versus those who did not, providing critical insights into risk factors and disease progression patterns.

Table 2: CKD Dataset: Comprehensive Patient Characteristics by ESRD Progression Status

Characteristic	ESRD Progression (n=86, 6.0%)	No ESRD Progression (n=1,336, 94.0%)	P-value
<b>Demographics</b>			
Age (years)	69.13 ± 12.37	72.04 ± 11.25	< 0.001
Female	40 (46.5%)	721 (54.0%)	0.215
Race			< 0.001
White	70 (81.4%)	1,242 (93.0%)	
African American	12 (14.0%)	60 (4.5%)	
Other	4 (4.6%)	34 (2.5%)	
BMI (kg/m <sup>2</sup> )	28.40 ± 5.32	26.40 ± 6.20	< 0.001
<b>Comorbidities</b>			
Diabetes	63 (73.3%)	788 (59.0%)	0.009
Hypertension	85 (99.0%)	1,323 (99.0%)	0.863
Cardiovascular Disease	10 (17.2%)	177 (18.2%)	0.990
Anemia	55 (64.0%)	828 (62.0%)	0.714
Metabolic Acidosis	22 (25.6%)	240 (18.0%)	0.077
Proteinuria	11 (12.8%)	227 (17.0%)	0.312
Secondary Hyperparathyroidism	28 (32.6%)	240 (18.0%)	< 0.001
Phosphatemia	4 (4.7%)	40 (3.0%)	0.390
Atherosclerosis	6 (9.4%)	149 (14.6%)	0.320
Heart Failure	6 (7.0%)	120 (9.0%)	0.526
Stroke	1 (1.2%)	40 (3.0%)	0.506
Conduction & Dysrhythmias	4 (4.7%)	214 (16.0%)	0.005
Myocardial Infarction	31 (51.7%)	316 (32.4%)	0.003
Fluid & Electrolyte Disorders	9 (17.6%)	122 (13.3%)	0.503
Metabolic Disorders	5 (9.4%)	60 (6.5%)	0.581
Nutritional Disorders	6 (10.2%)	106 (11.6%)	0.900
CKD Stage 4	47 (54.7%)	298 (22.3%)	< 0.001
CKD Stage 5	42 (48.8%)	277 (20.7%)	< 0.001

#### FEATURE CATEGORIES AND DESCRIPTIONS

The 38 clinical features in the CKD dataset are systematically organized across four major categories, each capturing distinct aspects of patient health and disease progression.

Table 3: CKD Dataset: Complete Feature Specifications

Category	Feature	Description
<b>Demographics</b>	Age	Patient age at baseline (years)
	Gender	Binary indicator (Male=0, Female=1)
	Race	Categorical encoding (White, Black, Hispanic, Other)
	BMI	Body Mass Index (kg/m <sup>2</sup> )
<b>Comorbidities</b>	Diabetes	Type 1 or Type 2 diabetes mellitus diagnosis
	Htn	Hypertension (systolic ≥140 or diastolic ≥90 mmHg)

Continued on next page

Table 3 – continued from previous page

Category	Feature	Description
	Cvd	Cardiovascular disease (coronary, cerebrovascular, peripheral)
	Anemia	Hemoglobin <13 g/dL (men) or <12 g/dL (women)
	MA	Mineral and bone disorders
	Prot	Proteinuria (>300 mg/day or >300 mg/g creatinine)
	SH	Secondary hyperparathyroidism
	Phos	Phosphorus disorders (hyperphosphatemia)
	Athsc	Atherosclerosis
	CHF	Congestive heart failure
	Stroke	Cerebrovascular accident history
	CD	Coronary disease
	MI	Myocardial infarction history
	FE	Iron deficiency
	MD	Metabolic disorders
	ND	Nutritional deficiency
	S4	CKD Stage 4 (eGFR 15-29 mL/min/1.73m <sup>2</sup> )
	S5	CKD Stage 5 (eGFR <15 mL/min/1.73m <sup>2</sup> )
<b>Lab Biomarkers</b>	Serum_Calcium	Serum calcium levels (mg/dL)
	eGFR	Estimated glomerular filtration rate (mL/min/1.73m <sup>2</sup> )
	Phosphorus	Serum phosphorus levels (mg/dL)
	Intact_PTH	Intact parathyroid hormone (pg/mL)
	Hemoglobin	Blood hemoglobin concentration (g/dL)
	UACR	Urine albumin-to-creatinine ratio (mg/g)
	Bicarbonate	Serum bicarbonate levels (mEq/L)
<b>Healthcare Utilization</b>	n_claims_DR	Number of durable medical equipment/drug claims
	n_claims_I	Number of inpatient claims
	n_claims_O	Number of outpatient claims
	n_claims_P	Number of physician service claims
	net_exp_DR	Net expenditure for DME/drugs (\$)
	net_exp_I	Net expenditure for inpatient services (\$)
	net_exp_O	Net expenditure for outpatient services (\$)
	net_exp_P	Net expenditure for physician services (\$)

#### STATISTICAL ANALYSIS AND CLINICAL SIGNIFICANCE

**Cohort Characteristics:** The complete cohort comprises 1,422 CKD patients with 24-month follow-up, yielding 8 temporal observations per patient (3-month intervals). ESRD progression occurred in 86 patients (6.0%), representing a clinically realistic progression rate for this advanced CKD population.

**Significant Risk Factors ( $p < 0.05$ ):** Statistical analysis revealed several key differentiators between ESRD progressors and non-progressors:

##### *Demographic Factors:*

- Younger age (69.1 vs 72.0 years) - counterintuitive finding suggesting more aggressive disease in younger patients
- Higher BMI (28.4 vs 26.4 kg/m<sup>2</sup>) - indicating metabolic burden
- Higher proportion of African Americans (14.0% vs 4.5%) - known ethnic disparity in CKD progression

##### *Comorbidity Profile:*

- Higher diabetes prevalence (73.3% vs 59.0%) - primary driver of CKD progression

Table 4: CKD Dataset: Laboratory Values and Healthcare Utilization by ESRD Progression Status

Feature	ESRD Progression (n=86)	No ESRD Progression (n=1,336)	P-value
<b>Laboratory Biomarkers</b>			
eGFR (mL/min/1.73m <sup>2</sup> )	17.21 ± 5.46	22.78 ± 5.66	< 0.001
Hemoglobin (g/dL)	12.15 ± 2.19	14.25 ± 1.80	< 0.001
Bicarbonate (mEq/L)	22.90 ± 6.36	25.30 ± 4.22	0.001
Serum Calcium (mg/dL)	9.39 ± 3.62	10.21 ± 2.86	0.042
Phosphorus (mg/dL)	3.61 ± 0.87	3.52 ± 0.72	0.350
Intact PTH (pg/mL)	78.66 ± 40.23	62.72 ± 37.32	0.001
<b>Healthcare Utilization Claims</b>			
Pharmacy Claims (count)	120 ± 94	109 ± 86	0.293
Inpatient Claims (count)	3.85 ± 3.41	3.74 ± 3.62	0.773
Outpatient Claims (count)	27.78 ± 24.75	22.07 ± 19.13	0.039
Professional Claims (count)	105.37 ± 77.56	87.43 ± 68.02	0.039
<b>Healthcare Expenditures (\$)</b>			
Pharmacy Expenditure	12,053 ± 11,596	10,440 ± 20,662	0.242
Inpatient Expenditure	33,909 ± 53,540	29,440 ± 32,541	0.446
Outpatient Expenditure	9,354 ± 17,522	8,554 ± 17,492	0.682
Professional Expenditure	15,512 ± 18,657	11,640 ± 12,748	0.061

- Increased secondary hyperparathyroidism (32.6% vs 18.0%) - marker of mineral bone disorder
- More myocardial infarction (51.7% vs 32.4%) - cardiovascular complications
- Paradoxically lower conduction disorders (4.7% vs 16.0%) - may reflect survival bias
- Higher CKD stage 4 (54.7% vs 22.3%) and stage 5 (48.8% vs 20.7%) prevalence

#### Laboratory Markers:

- Significantly lower eGFR (17.2 vs 22.8 mL/min/1.73m<sup>2</sup>) - expected primary marker
- Lower hemoglobin (12.2 vs 14.3 g/dL) - indicating CKD-related anemia
- Lower bicarbonate (22.9 vs 25.3 mEq/L) - metabolic acidosis marker
- Higher intact PTH (78.7 vs 62.7 pg/mL) - secondary hyperparathyroidism
- Lower serum calcium (9.4 vs 10.2 mg/dL) - mineral bone disorder

#### Healthcare Utilization:

- Higher outpatient claims (27.8 vs 22.1) - increased monitoring needs
- Higher professional claims (105.4 vs 87.4) - specialist consultations

## A.2 MIMIC-IV DATASET CHARACTERISTICS

### COHORT CONSTRUCTION AND SELECTION CRITERIA

The MIMIC-IV cohort was constructed through a systematic pipeline designed to ensure data quality and clinical relevance for mortality prediction tasks.

#### Initial Database Statistics:

- Total ICU stays in MIMIC-IV: 94,458
- Unique patients: 65,366
- Multiple ICU stays per patient: 29,092 additional stays

**Cohort Construction:** Our preprocessing pipeline selects the first ICU stay per patient to ensure independence of observations, resulting in exactly 65,366 patients. This approach eliminates potential confounding from repeated admissions while maintaining a substantial sample size for robust model training and evaluation.

**Final Cohort:** 65,366 patients meeting all inclusion criteria.

#### FEATURE STATISTICS

Table 5 presents detailed statistics for all MIMIC-IV features, including percentile distributions to capture the full range of physiological values encountered in critical care.

Table 5: MIMIC-IV Dataset: Comprehensive Feature Statistics (n=65,366 patients)

Feature	Mean $\pm$ SD	Median [IQR]	Missing (%)
<b>Demographics</b>			
Age (years)	64.5 $\pm$ 17.1	66.0[54.0, 78.0]	0.0
Gender (Female %)	43.8%	-	0.0
<b>Vital Signs</b>			
Heart Rate (bpm)	84.1 $\pm$ 18.9*	82.0[71.0, 95.0]	27.5
Systolic BP (mmHg)	119.9 $\pm$ 25.8*	117.0[104.0, 133.0]	51.6
Diastolic BP (mmHg)	67.4 $\pm$ 15.8*	64.0[55.0, 75.0]	51.6
Mean BP (mmHg)	87.6 $\pm$ 16.9*	78.0[69.0, 89.0]	51.6
Respiratory Rate (rpm)	22.7 $\pm$ 6.8*	19.0[15.0, 22.0]	28.4
Temperature ( $^{\circ}$ C)	37.0 $\pm$ 0.8	36.8[36.6, 37.2]	81.3
SpO2 (%)	96.8 $\pm$ 3.2*	97.0[95.0, 99.0]	28.9
<b>Laboratory Tests</b>			
Creatinine (mg/dL)	1.4 $\pm$ 1.5	1.0[0.7, 1.5]	93.1
Glucose (mg/dL)	141.1 $\pm$ 69.7	125.0[103.0, 157.0]	93.5
Sodium (mEq/L)	138.2 $\pm$ 5.6	138.0[135.0, 141.0]	92.9
Potassium (mEq/L)	4.2 $\pm$ 0.7	4.1[3.8, 4.5]	92.8
Hematocrit (%)	31.1 $\pm$ 6.0	30.5[26.7, 35.1]	92.3
WBC (K/ $\mu$ L)	12.3 $\pm$ 10.7	10.7[7.8, 14.7]	93.3

*Note: \* indicates features with outliers present in raw data that require preprocessing. Standard deviations shown are after outlier detection but before winsorization.*

**Outlier Detection and Treatment:** Physiologically implausible values are identified using clinical knowledge-based thresholds and statistical methods:

- Heart Rate: <20 or >220 bpm
- Blood Pressure: Systolic <50 or >250 mmHg, Diastolic <20 or >150 mmHg
- Temperature: <32 $^{\circ}$ C or >42 $^{\circ}$ C
- SpO2: <70% or >100%
- Laboratory values: Beyond 99.5th percentile of physiologically reasonable ranges

Outliers are winsorized to the 1st and 99th percentiles to preserve distributional properties while reducing the impact of measurement errors.

**Normalization:** All continuous features are standardized using z-score normalization:  $z = \frac{x-\mu}{\sigma}$ , where  $\mu$  and  $\sigma$  are computed on the training set only to prevent data leakage.

## COHORT CHARACTERISTICS AND OUTCOMES

Table 6: MIMIC-IV Cohort: Clinical Characteristics and Outcomes

<b>Characteristic</b>	<b>Value</b>	<b>Percentage</b>
Total Patients	65,366	-
Age Distribution		
Mean Age	64.5 ± 17.1 years	-
Age Range	18-103 years	-
Gender		
Male	36,720	56.2%
Female	28,646	43.8%
Temporal Structure		
Observation Window	48 hours	Hourly resolution
Total Observations	3,137,568	(65,366 × 48)
Features per Patient	15	7 vitals + 6 labs + 2 demographics
<b>Clinical Outcomes</b>		
Hospital Mortality	7,086	10.8%
Survivors	58,280	89.2%
<b>Data Quality Characteristics</b>		
Vital Signs Missing Data	27.5-81.3%	Variable by feature type
Laboratory Tests Missing Data	92.3-93.5%	Expected for ICU setting
Demographics Missing Data	0.0%	Complete for all patients

## B DATA PROCESSING IMPLEMENTATION DETAILS

### B.1 MIMIC-IV PREPROCESSING PIPELINE

The preprocessing pipeline for MIMIC-IV data involves several computational steps designed to handle the scale and complexity of the raw database:

**Computational Requirements:**

- Memory usage: ~32GB RAM for full dataset processing
- Processing time: ~4-6 hours on 16-core CPU
- Storage: Raw data (120GB), processed data (8.2GB)

**Batch Processing Strategy:** To manage memory constraints, patient processing is batched in groups of 1,000 patients, with relevant chartevents and labevents filtered for each batch to minimize memory footprint.

**Temporal Alignment:** All timestamps are aligned to ICU admission time (intime), with measurements indexed by hour offset (0-47) from admission. This standardization enables consistent temporal modeling across patients.

### B.2 FEATURE ENGINEERING CONSIDERATIONS

**Clinical Rationale for Feature Selection:**

- **Vital Signs:** Selected based on immediate availability and prognostic value in ICU mortality prediction
- **Laboratory Tests:** Chosen to represent major organ systems (kidney, metabolism, hematology, infection)
- **Exclusions:** Medication and intervention data excluded to focus on physiological state rather than treatment effects

**Temporal Binning Strategy:** Measurements within each hour are aggregated using median values to reduce noise while preserving clinical trends. This approach balances temporal resolution with data stability.

## C HYPERPARAMETER CONFIGURATION DETAILS

This appendix provides comprehensive hyperparameter details for four key models evaluated on the Chronic Kidney Disease (CKD) progression prediction task: BiLSTM, RETAIN, StageNet, and Chain-of-Influence (CoI). For each model, we present both the search space of hyperparameter candidates and the optimal configuration identified through hyperparameter optimization.

### C.1 BiLSTM (BIDIRECTIONAL LONG SHORT-TERM MEMORY)

#### HYPERPARAMETER SEARCH SPACE

Hyperparameter	Candidates
Batch Size	{16, 32, 64}
Dropout Rate	{0.1, 0.2, 0.3}
Hidden Dimension	{64, 128, 256}
Learning Rate	{0.0001, 0.001, 0.01}
Number of Layers	{1, 2, 3}

Table 7: BiLSTM hyperparameter search space (Total:  $3 \times 3 \times 3 \times 3 \times 3 = 243$  combinations)

#### OPTIMAL CONFIGURATION

Hyperparameter	Best Value
Batch Size	128
Dropout Rate	0.2
Hidden Dimension	32
Learning Rate	0.001
Number of Layers	2

Table 8: BiLSTM optimal hyperparameters

## C.2 RETAIN (REVERSE TIME ATTENTION)

## HYPERPARAMETER SEARCH SPACE

Hyperparameter	Candidates
Batch Size	{16, 32, 64}
Dropout Rate	{0.1, 0.2, 0.3}
Embedding Dimension	{32, 64, 128}
Hidden Dimension	{64, 128, 256}
Learning Rate	{0.0001, 0.001, 0.01}
Number of Attention Heads	{4, 8, 16}
Number of Layers	{2, 3, 4}

Table 9: RETAIN hyperparameter search space (Total:  $3 \times 3 \times 3 \times 3 \times 3 \times 3 \times 3 = 2187$  combinations)

## OPTIMAL CONFIGURATION

Hyperparameter	Best Value
Batch Size	64
Dropout Rate	0.0
Embedding Dimension	16
Hidden Dimension	32
Learning Rate	0.001
Number of Attention Heads	8
Number of Layers	3

Table 10: RETAIN optimal hyperparameters

## C.3 STAGENET (STAGE-AWARE NEURAL NETWORK)

## HYPERPARAMETER SEARCH SPACE

Hyperparameter	Candidates
Batch Size	{32, 64, 128}
Dropout Rate	{0.1, 0.2, 0.3}
Hidden Dimension	{64, 128, 256}
Learning Rate	{0.0001, 0.001, 0.01}
Number of Stages	{3, 4, 5}
Kernel Size	{3, 5, 7}

Table 11: StageNet hyperparameter search space (Total:  $3 \times 3 \times 3 \times 3 \times 3 \times 3 = 729$  combinations)

## OPTIMAL CONFIGURATION

Hyperparameter	Best Value
Batch Size	128
Dropout Rate	0.2
Hidden Dimension	512
Learning Rate	0.0001
Number of Stages	5
Kernel Size	5

Table 12: StageNet optimal hyperparameters

## C.4 COI (CHAIN-OF-INFLUENCE WITH DYNAMIC TANH NORMALIZATION)

## HYPERPARAMETER SEARCH SPACE

Hyperparameter	Candidates
Batch Size	{128}
Dropout Rate	{0.0, 0.2, 0.4}
Embedding Dimension	{16, 32, 64}
Hidden Dimension	{32, 64, 128}
Learning Rate	{0.001, 0.0001}
Number of Attention Heads	{2, 4, 8}
Number of Layers	{2, 4, 6}
Alpha Initialization	{0.8} ( <i>DyT-specific</i> )

Table 13: CoI hyperparameter search space (Total:  $1 \times 3 \times 3 \times 3 \times 2 \times 3 \times 3 \times 1 = 486$  combinations)

## OPTIMAL CONFIGURATION

Hyperparameter	Best Value
Batch Size	128
Dropout Rate	0.2
Embedding Dimension	16
Hidden Dimension	128
Learning Rate	0.0001
Number of Attention Heads	2
Number of Layers	8
Alpha Initialization (DyT)	0.8

Table 14: CoI optimal hyperparameters

## C.5 TRAINING CONFIGURATION

All models were trained with the following common settings:

Parameter	Value
Maximum Epochs	500
Early Stopping Patience	7
Optimizer	Adam
Loss Function	BCEWithLogitsLoss
Validation Split	20%
Test Split	20%
Random Seed	42

Table 15: Common training configuration for all models